Tau Aggregation Correlates with Amyloid Deposition in Both Mild Cognitive Impairment and Alzheimer's Disease Subjects

DOI:
10.3233/JAD-181168

Document Version
Accepted author manuscript

Manuscript

Tau aggregation correlates with amyloid deposition in both mild cognitive impairment and Alzheimer's disease subjects.

Running title: Tau and amyloid aggregation in MCI and AD

Melanie Dani MRCP[a], Melanie Wood MRCP[a], Ruth Mizoguchi FRCP[a], Zhen Fan MSc[a], Trudi Edginton PhD[b], Rainer Hinz PhD[c], Zarni Win MRCP FRCR[d], David James Brooks FRCP DSc FMedSci[a,e,f], Paul Edison MD, MRCP, PhD, FRCP, FRCPI [a]

a) Neurology Imaging Unit, Department of Medicine, Imperial College London, DuCane Rd, London, W12 0NN, UK
b) Department of Psychology, City University of London, EC1R 0JD
c) Wolfson Molecular Imaging Centre, University of Manchester,27 Palatine Road, Manchester M20 3LJ, UK
d) Imperial College Healthcare NHS Trust, Charing Cross Hospital, Fulham Palace Road, London, UKW6 8RF
e) Department of Nuclear Medicine, Aarhus University, Nordre Ringgade 1, 8000 Aarhus, Denmark
f) Institute of Neuroscience, University of Newcastle upon Tyne, Newcastle University Campus for Ageing and Vitality
Newcastle NE4 5PL UK

Corresponding author:

Dr Paul Edison MD, MRCP, PhD, FRCP, FRCPI

Neurology Imaging Unit

Division of Brain Sciences

Imperial College London

DuCane Road, Hammersmith Hospital, London, W12 0NN

UK

Tel: +44 203 383 3725

Fax: +00 44 203 313 4320

Email: paul.edison@imperial.ac.uk

Keywords:

Alzheimer's, mild cognitive impairment, tau, amyloid, PET

Word counts:

Paper: 3355 words, Abstract: 167 words, References: 34; 3 tables, 3 figures, 3 supplementary figures

Abstract

Background

Amyloid plaque and tau-containing neurofibrillary tangles are important features of Alzheimer's Disease (AD). However, the relationship between these processes is still debated.

Objective

We aimed to investigate local and distant relationships between tau and amyloid deposition in the cortex in Mild Cognitive Impairment (MCI) and AD using PET imaging.

Methods

Seventy-nine subjects (fifty-one controls, thirteen amyloid-positive MCI subjects and fifteen amyloid positive AD subjects) underwent MRI and ^{18}F-flutemetamol PET. All MCI/AD subjects and eight healthy controls as well as thirty-three healthy control subjects from the ADNI dataset also had ^{18}F-AV1451 PET. Regional and distant correlations were examined after sampling target-to-cerebellar ratio images. Biological parametric mapping was used to evaluate voxel level correlations locally.

Results

We found multiple clusters of voxels with highly significant positive correlations throughout the association cortex in both MCI and AD subjects.

Conclusion

The multiple clusters of positive correlations indicate that tau and amyloid may interact locally and be involved in disease progression. Our findings suggest that targeting both pathologies may be required for an effective treatment.

Introduction

Amyloid β (Aβ) plaques and tau-containing neurofibrillary tangles (NFTs) have been consistently described as cardinal features of Alzheimer's disease (AD)[1]. While the presence of both is required for a pathological diagnosis of AD, the exact interaction is still debated.

Aβ has a central role in AD: by definition, plaques are necessary but not sufficient for a diagnosis of AD [2]. NFTs are also required for a diagnosis [1]. However, NFT aggregation increases with age almost universally, but can occasionally be found in healthy individuals under 30 years [3, 4]. Thus, isolated medial temporal tauopathy is not sufficient to cause AD [4]. This suggests that while Aβ plaques and tau tangles are both required to cause AD, neither is sufficient by itself.

PET imaging allows us to evaluate both these processes. ^{18}F-flutemetamol and ^{18}F-florbetapir are amyloid tracers, while ^{18}F-AV1451 has nanomolar affinity for paired helical filament-tau[5]. PET also enables us to correlate these processes at a voxel level using biological parametric mapping (BPM) analysis in SPM[6].

We hypothesised that tau aggregation would correlate at voxel level with amyloid levels in the isocortex, and that tau aggregation in the medial temporal lobe structures would correlate with amyloid in the isocortex. We further hypothesised that there will be local correlation between tau and amyloid in different cortical regions.

Methods

Standard Protocol Approvals, Registrations and Patient Consents

Ethical approval was obtained from local and national ethics committees (The Riverside Research Ethics Committee – National Health Research Services, Health Research Authority,

UK.) The approval for administration of radioactive activity was given by the Administration of Radioactive Substances Advisory Committee (ARSAC). Written informed consent was obtained from all subjects.

Recruitment

Subjects were recruited from memory clinics, a national dementia recruitment website and advertisements in local media. All subjects underwent a screening visit consisting of history, physical and neurological examination and neuropsychological testing. The clinical diagnosis of MCI or AD was re-confirmed applying the Petersen[7] and NINCDS-ADRDA (National Institute of Neurological and Communicative Disorders and Stroke and the Alzheimer's disease and Related Disorders Association (NINCDS-ADRDA) criteria, respectively [8, 9].

Inclusion criteria were: 1) A diagnosis of MCI as defined by the Petersen criteria, or AD as defined by NINCDS-ADRDA criteria, or normal cognition for the healthy controls. 2) Age range 50-85 years. 3) Ability to give informed consent. 4) At least 8 years of formal education. 5) MMSE above 24 for MCI, above 15 for AD, and normal cognition for healthy control subjects. Exclusion criteria were: 1) Major depression, or any significant disease influencing neuropsychological testing. 2) A history of schizophrenia/schizoaffective disorder. 3) Contraindication to MRI scanning. 4) A malignancy within the last 5 years.

ADNI database

In order to ensure a sufficiently large group of normal controls (only eight controls from our centre had ^{18}F-AV1451 scans), thirty- three healthy control subjects were drawn from the ADNI database (http://adni.loni.usc.edu/). Selection criteria included subjects who had had amyloid and tau imaging, and age range between 65-75 years old. All subjects gave written informed consent.

Image acquisition

ADNI controls

A description of the MRI, ^{18}F-AV45 and ^{18}F-AV1451 data acquisition for the thirty-three controls from the ADNI database is available on the ADNI website (http://www.adni-info.org/Scientists/ADNIStudyProcedures.aspx). Only the ^{18}F-AV1451 scans for these individuals were used in the correlation and group analyses, as these individuals had different amyloid PET scans from our cohort (^{18}F-florbetapir scans were used in the ADNI controls, and ^{18}F-flutemetamol used in our centre).

MRI

Subjects recruited at our centre had Magnetic Resonance Imaging (MRI) with a 3 Tesla Siemens 32-channel Verio scanner. A T1-weighted magnetisation prepared rapid gradient echo sequence (MPRAGE; time repetition = 2400 ms, time echo = 3.06 ms, flip angle of 9, inversion time = 900 ms, matrix = [256 x 246]) with a 1 mm^3 voxel size, anteroposterior phase encoding direction, and a symmetric echo was used. Two subjects with coronary artery stents (who were ineligible for 3 Tesla MRI) underwent 1.5 Tesla MRI in a Philips Achieva system (Best, Netherlands) at the MRC Clinical Sciences Centre, Imperial College London.

^{18}F-flutemetamol

^{18}F-flutemetamol was manufactured by GE Healthcare, Amersham, UK, and scans were performed at Imperial College Clinical Imaging Facility using a Siemens Biograph 6 scanner with a 15cm field of view. A mean dose of 183.4(±5.3) MBq ^{18}F-flutemetamol in 8ml saline was injected followed by a 5-10ml saline flush. Data was acquired in 3D list mode from 90 to 120 minutes following injection and re-binned as 6x5 minute frames. Image reconstruction was performed by filtered back projection with attenuation correction. Post reconstruction 5mm Gaussian smoothing was applied (The zoom was 2.6, the matrix size was 168x168 and the pixel size was 1.56mm x 1.56mm x 1.92mm).

^{18}F-AV1451 (flortaucipir)

^{18}F-AV1451 was manufactured at Imanova Centre for Imaging Sciences, London, and scans were acquired using a Siemens Truepoint PET/CT (axial field of view of 21.8cm; 111 transaxial planes; spatial resolution of 2.056mm x 2.056 mm x 2 mm after image reconstruction. A mean dose of 168.3(±7.4) MBq ^{18}F-AV1451 in 20 ml saline was injected. Data was acquired in 3D list mode for 120 minutes and the data was rebinned at the following time frames: 8x15 seconds, 3x 60 seconds, 5x120 seconds, 5x300 seconds, 8x600 seconds. Data reconstruction was performed by iterative reconstruction and 5mm Gaussian smoothing post reconstruction.

Image processing

Image processing was performed with Analyze AVW 11.0 and SPM (Statistical parametric mapping software; Wellcome Trust Centre for Neuroimaging, University College London) on a Matlab platform. Scans were pre-processed in Analyze AVW. Voxel level correlations were performed using the Biological Parametric Mapping toolbox, which is integrated into SPM5 software. Regional correlations were calculated using SPSS version 24.0 (IBM), using a statistical threshold of significance of 0.05.

Creation of ratio images for ^{18}F-flutemetamol and ^{18}F AV1451

The 90-120 minute summed PET image for ^{18}F-flutemetamol and 80-100 minute summed PET image for ^{18}F-AV1451 were co-registered to the T1-weighted MRI and were then transformed into standard Montreal Neurologic Institute (MNI) space. In order to create an object map for each subject, each individual MRI was segmented in Analyze AVW into grey matter, white matter and cerebrospinal fluid (CSF). Grey matter voxels were those that had a >50% probability of containing grey matter and were used to create an individual grey matter binarised image. This individual grey matter binarised image was then convolved with the

Hammers probabilistic atlas[10] to create an individualised object map. This object map was then applied to the normalised PET to quantify the uptake in the cerebellum. RATIO images were then created by dividing the individual PET image by the uptake of cerebellar grey matter to create a target to cerebellar RATIO image. The ratio image was then sampled for individual regions.

Voxel level examination of tracer binding

SPM8 was used to perform independent t-tests on the data (p-value <0.05, no extent threshold) to distinguish voxel level tracer uptake between the MCI/AD groups and the control group, using the normalised ratio images for ^{18}F-AV1451 and ^{18}F-flutemetamol.

Creation of Z-score maps and voxel-level correlations using biological parametric mapping

Voxel level correlations between ^{18}F-AV1451 and ^{18}F-flutemetamol were examined using the biological parametric mapping toolbox in SPM written on a Matlab (Mathworks Inc) platform[6]. Z-score maps were created for each subject, for each tracer, to demonstrate the specific increase in tracer uptake compared to the control group. Generating a Z-score parametric map allows multi-modal comparison of different tracers, representing the level of each pathology relative to the control group. In addition, it accounts for non-specific binding seen in these tracers. The Z-score was calculated using the following formulae:

Z score [^{18}F-flutemetamol] *= (^{18}F-flutemetamol ratio image of patient– mean ^{18}F-flutemetamol ratio image of control group)/standard deviation of ^{18}F-flutemetamol ratio image for control group*

Z score [^{18}F-AV1451] *= (^{18}F-AV1451 ratio image of patient– mean ^{18}F-AV1451 ratio image of control group)/standard deviation of ^{18}F-AV1451 ratio image control group*

Individual Z-score ^{18}F-flutemetamol and ^{18}F-AV-1451 maps were then interrogated in BPM toolbox in order to localise clusters of positive correlation between the uptake of the two tracers. Results were corrected for family wise error. All clusters with a corrected p-value of $p<0.05$ with an extent threshold of 1000 voxels were considered significant.

Single subject SPM analysis

Individualised tracer uptake on a 'single subject' basis was performed using an independent t-test in SPM, compared to the control group. This allowed us to identify clusters of significantly increased tracer uptake in each individual.

Region of interest analysis

Region of interest (ROI) analysis of the RATIO images was performed by sampling the following regions - anterior cingulate, posterior cingulate, temporal, frontal, parietal and occipital lobes. Correlations were considered significant if the p-value was < 0.05. Group comparisons were examined using the Kruskal-Wallis test. Regional correlations were interrogated using Spearman rho correlation coefficient, using continuous variables (SUVR values for ^{18}F-flutemetamol and ^{18}F-AV1451 for each region). Spearman rho correlation coefficient was used rather than Pearson coefficient because of the small number of participants used in the study.

Only MCI and AD subjects with positive amyloid scans were included in this study, because we wanted to examine the relationship between increasing amyloid load and tau deposition. Furthermore, we wanted to examine the underlying processes in individuals on the AD trajectory. Amyloid status was defined as positive if there was binding above the recently published cut-off of SUVR 1.42 in one or more of the regions described above (anterior cingulate, posterior cingulate, frontal, temporal, parietal and occipital lobes).[11] Tau status was considered positive if binding was above the threshold of 1.32 in the temporal lobe

structures (hippocampus, parahippocampus, amygdala, fusiform gyrus), whole temporal lobe, parietal, frontal or occipital lobe. [11]

Results

Demographics

In total, seventy-nine subjects participated in the study (fifty-one healthy controls, thirteen amyloid-positive MCI subjects and fifteen amyloid-positive AD subjects). Eighteen controls were recruited at our centre at Imperial College London (all had ^{18}F-flutemetamol and eight of these had ^{18}F-AV1451 scans). Additionally the scans of thirty-three healthy controls were used from the ADNI database for ^{18}F-AV1451 (these participants also had MMSE, MRI scans and ^{18}F-AV45 (^{18}F-florbetapir scans). Subjects recruited from our centre had neuropsychometric testing, T1-weighted MRI and ^{18}F-flutemetamol. Table 1a shows the age and MMSE scores for the cohort. Table 1b shows the neuropsychometric data for the subjects recruited at our centre.

Voxel level increases in tau aggregation and amyloid deposition in MCI and AD

Figure 1 shows the voxel-level increases in ^{18}F-flutemetamol and ^{18}F-AV1451 in the MCI and AD groups compared to the controls

We were interested particularly in the relationships and correlations in the MCI group, and so we examined the spatial distribution of amyloid and tau in each individual MCI subject. Figure 2 shows the distribution of amyloid and tau aggregation in the six MCI individuals who had voxel level significant increases in tau aggregation compared with the controls on independent t-test. The amount and density of both amyloid deposition and tau aggregation varied in these MCI individuals, demonstrating the heterogeneity of the pathological load in these individuals.

Regional level increases in amyloid and tau in MCI and AD

Individual SUVR values for each subject are shown in Supplementary Figures 1 (for ^{18}F-Flutemetamol), Supplementary Figure 2 (for ^{18}F-AV1451) and Supplementary Figure 3 (individuals recruited from the ADNI database). Both the MCI and AD groups demonstrated significantly increased ^{18}F-flutemetamol uptake in the fusiform gyrus, anterior and posterior cingulate cortex, temporal frontal, parietal and occipital cortices. (Supplementary Table 1)

The AD group had significantly higher ^{18}F-AV1451 retention in the hippocampus, fusiform gyrus, amygdala, parahippocampus, temporal, frontal, parietal and occipital cortices. The MCI group had higher ^{18}F-AV1451, retention than the controls in the hippocampus, fusiform gyrus, amygdala, and parahippocampus. (Supplementary Table 2)

Voxel level correlations between amyloid and tau aggregation in the cortex

There were multiple clusters of highly significant positive correlations between ^{18}F-AV1451 and ^{18}F-Flutemetamol in both MCI and AD (shown in Figure 3 and Table 2). In the MCI group, the clusters of strongest correlation (that is Z-scores over 4) were in the frontal and temporal cortices, and subcortical structures (corpus callosum, thalamus and caudate). In the AD group the largest clusters of strong correlation were in the frontal lobe. Z-scores and correlation coefficients were higher in the positive correlation clusters in the MCI group compared with those in the AD group.

Regional level correlations between amyloid and tau aggregation in the cortex

In the AD group, there was a positive correlation in the amygdala ($r=0.588$, $p=0.035$) but no correlations in the MCI group.

Discussion

This is the first study to our knowledge to examine *in vivo* voxel level correlations between amyloid deposition and tau aggregation in MCI subjects compared with AD subjects. We found highly significant clusters of positive correlations throughout the cortex in both MCI and AD. Z-scores and r correlation coefficients were higher in the MCI group than the AD group, which may be due to the plateauing of amyloid deposition at the MCI stage, while NFT aggregation continues to intensify as the disease progresses [2, 12, 13].

At a regional level, we did not find correlations either locally or in cortical projections in the MCI group. In the AD group, there were correlations in the amygdala only. This was an unexpected finding, and possibly reflects the heterogeneity of the disease process, particularly at the MCI stage. Our groups may have been underpowered to detect the differences in the processes and correlations. Finally, it is possible that the regions that we were analysing were too large to detect voxel level processes.

Our findings are in line with histopathological findings of AD brains showing that amyloid and tau coexist within neurons in AD [14] consistent with the voxel-level correlations seen in our study. It is possible that the two processes occur independently, but in close proximity to each other, as tau propagation both locally and across the cortex can occur independently of amyloid. [15]

There is evidence, however, that the processes act synergistically in driving disease progression. Tau transgenic (rThTauEC) mice (which overexpress tau in the medial temporal lobe) crossed with amyloid transgenic mice (APP/PS1) show a significantly higher tau load with propagation throughout the cortex when cortical Aβ is present[16]. Injecting brain extracts from amyloid transgenic mice into tau transgenic mice results in spreading of tau from the hippocampus to projection at more distant sites. In human neural cell cultures, inhibition of Aβ formation reduces tauopathy [17] further implicating amyloid in inducing

tau aggregation. The voxel level correlations, suggesting local aggregation, may also point to local toxicity between the two processes. In vitro studies have shown that Aβ induces tau fibrillisation by cross-seeding, and enhances existing tau aggregation. The possibility of this process occurring across specific networks could explain the spatial discordance between these two pathologies [18], networks involving the hippocampus providing a transport mechanism for tau while those involving the cingulate transport Aβ aggregates.

Similarly, tau can promote amyloid pathology. The presence of tau aggregates can enhance Aβ toxicity[19], which in turn exerts its toxicity by neuronal projections. Injecting phosphorylated tau from AD brains into transgenic AD mice (3xTg; mutations to APP, Presenilin 1 and MAPT 1) not only induced tau aggregation and propagation, but also increased amyloid plaque load (compared with injection of saline). [20] The same group found that passive immunisation of monoclonal antibodies to tau into AD transgenic mice not only decreased total tau and phosphorylated tau, but also decreased amyloid precursor protein (APP) levels and amyloid plaque.[21] This suggests that passive immunisation to tau could target both pathologies, thus breaking the disease cycle and halting disease progression.

In humans, it is suggested that isocortical amyloid may be required to induce slow developing medial temporal lobe NFTs to become rapidly spreading toxic NFT aggregates in the isocortex [22, 23]. Thus, while the processes can appear to be spatially discordant, there may be multiple neuronal projections connecting these ‘discordant’ areas. For example, corticocortical evoked potential studies in humans have revealed connections between the hippocampus and temporal lobe structures; the parahippocampus and posterior cingulate cortex; and between the amygdala and the temporal, frontal, inferior parietal, cingulate, and insula [24]. Evoked intracranial EEG responses in humans have suggested multiple connections between lobes – with a high frequency of connections within the temporal and frontal lobes[25].

It is likely that while these processes can occur independently, they also act synergistically and have been described as a 'toxic *pas de deux*'. [26]

Study strengths and limitations

A strength of this study was that our individuals with MCI and AD were well characterised and showed amyloid positivity on PET. This allowed us to evaluate tau aggregation in homogenous groups of individuals. Additionally, interrogation for both regional and voxel-level correlations revealed the full extent of spatial associations between the two processes.

A limitation of the study was the inclusion of small numbers of individuals in each disease group, so caution needs to be applied when we generalise our results to the MCI and AD populations. Additionally, the inclusion of both tau positive and tau negative MCI individuals in the correlation analysis introduces the possibility of false positive results arising from null data points. If we had larger numbers we would have performed separate correlation analyses for tau-positive and all patients, respectively. However, we felt that it was important to include all individuals in this case, as tau deposition is a continuous process in the AD trajectory.

Another consideration is the reported off-target binding of ^{18}F-AV1451 described in the choroid plexus, basal ganglia, retinal tissue and melanin containing cells[27-29] so our results should be interpreted with caution. However, the use of individualised Z-maps reduces this problem. While our findings are in line with previous histopathological studies [14], ideally our findings should be confirmed with autoradiographic studies. Additionally, detection of correlated tracer binding is influenced by the sensitivity of PET radioligands and is liable to false negatives [30]. Amyloid PET imaging can only confidently detect amyloid plaques at Thal stage 3 or higher when the load is moderate or severe and consistently misses Thal stages 1 and 2. Individuals who are labelled as amyloid negative PART (Primary-age related

tauopathy) based on PET imaging may have Aβ that is below the threshold for detection[30]. Alternatively, they may enter an amyloidogenic pathway after NFTs aggregate in the medial temporal lobes [31, 32]. Another consideration is our chosen cut-offs for amyloid and tau positivity, based on previous models by Jack et al. [11] Amyloid and tau deposition are continuous processes. In particular, tau deposition increases in the medial temporal lobes in normal ageing, and thresholds for biomarker positivity are still debated. Thus, positivity depends on the threshold used. Additionally, both amyloid and tau can be present in healthy controls.[33, 34]. In view of the limited numbers and the older age of the cohort, we did not differentiate between preclinical AD stages 0, 1 and 2 when creating Z-scores for our disease groups. If we had only used individuals with preclinical AD stage 0, higher levels of tracer uptake in the MCI and AD group would be likely.

Additionally, we included a subset of ^{18}F-AV1451 scans for healthy controls recruited from the ADNI database. These individuals had amyloid scans, but using a different tracer from our centre (^{18}F-florbetapir, compared to ^{18}F-flutemetamol) so direct comparison of amyloid was not possible. Additionally, the ^{18}F-AV1451 scans were performed on different scanners, increasing the possibility of introducing variability into the cohort.

Here we report for the first time that correlations between amyloid and tau are stronger in MCI compared with AD. This is consistent with the fact that both pathologies are increasing in MCI but then amyloid deposition plateaus, while NFT aggregation continues to progress with the clinical course. However, a longitudinal study would allow us to better establish the temporal relationship between these processes, and the sequence of events.

Conclusion

In this PET study of MCI and AD subjects, we found that amyloid deposition and tau aggregation were significantly correlated at a voxel level across association cortex, in both

MCI and AD. Our findings reinforce the view that the two pathological processes are synergistic when contributing to AD. The strong correlations in the MCI group may suggest that both these pathological processes are still evolving in the MCI stage. Any future therapeutic strategy may need to target both of these pathologies.

Tables

Table 1a Demographic data of study participants. Values are mean (standard deviation)

	Controls	**MCI**	**AD**
Age	70.68(7.57)	76.08(5.15)	72.10(7.40)
MMSE	29.44(1.05)	28.15(1.21)	21.87(3.58)

Table 1b Neuropsychometric data of the subjects recruited at our centre. Values are mean (standard deviation) *** p<0.05, ** p<0.01**

Test	**Controls (n=18)**	**MCI (n=13)**	**AD (n=15)**
Rey delayed	18.18(7.12)	9.58(7.35)*	3.67(5.59)**
Logical delayed	27.36(5.94)	10.11(5.32)**	4.46(5.99)**
Hopkins delayed recall	10.15(2.11)	2.31(1.75)**	1.46(1.90)**
Hopkins Recognition Index	11.29(1.07)	7.54(3.02)**	4.54(3.43)**
Semantic fluency	21.00(6.13)	14.23(4.09)**	11.85(5.43)**
Verbal fluency	49.36(10.80)	39.92(10.84)	34.08(14.85)**
Digit span	19.07(3.45)	18.38(7.01)	13.46(4.72)*
Letter number sequencing	11.08(3.09)	7.15(2.41)**	4.62(3.48)**
Trail Making A	35.54(11.17)	61.23(29.73)	112.82(125)*
Trail Making B	71.50(21.39)	186.54(110.57)**	165.33(69)*

Table 2 Voxel level correlations between ^{18}F-flutemetamol and ^{18}F-AV1451 in MCI and AD

Region	Coordinates	Z-score	R correlation coefficient	p-value	Cluster size
Left presubgenual frontal cortex	-1 37 -7	5.23	0.970	<0.00001	170741
Corpus callosum	-6 25 -3	5.17	0.970		
Right middle frontal gyrus	18 43 -9	4.96	0.960		
Left middle frontal gyrus	-17 32 4	4.85	0.960		
Right thalamus	8 -4 4	4.58	0.940		
Right presubgenual frontal cortex	6 32 -4	4.49	0.940		
Left caudate nucleus	-15 12 8	4.46	0.930		
Left posterior temporal lobe	-26 -34 6	4.37	0.930		
Right subgenual frontal cortex	1 29 -6	4.33	0.930		
Left putamen	-16 6 -7	4.3	0.920		
Left thalamus	-16 -18 2	4.08	0.910		
Left insula	-23 20 6	4.02	0.900		
Left middle frontal gyrus	-53 21 29	3.54	0.850	<0.00001	25919
Left inferior frontal gyrus	-56 33 10	3.25	0.820		
Left precentral gyrus	-50 -2 40	3.15	0.800		
Left superior frontal gyrus	-15 59 35	3.12	0.800		

Left superior temporal gyrus anterior part	-60 4 -12	3.71	0.870	<0.00001	11721
Left insula	-41 -1 -9	2.76	0.740		
Left postcentral gyrus	-66 -12 22	2.62	0.720		
Left middle and inferior temporal gyrus	-69 -16 -14	2.55	0.700		
Left superior temporal gyrus, posterior part	-53 0 -8	2.4	0.670		
Left anterior temporal lobe, lateral part	-58 8 -27	2.2	0.630		
Left postcentral gyrus	-60 -16 34	1.98	0.580		
Right superior frontal gyrus	18 -11 58	4.24	0.920	0.030	6020
Right precentral gyrus	29 -13 51	3.19	0.810		
Alzheimer's disease					
Left middle frontal gyrus	-22 21 11	4.34	0.900	<0.00001	173296
Right posterior temporal lobe	28 -35 -3	4.29	0.890		
Left caudate nucleus	-16 15 9	4.28	0.890		
Corpus callosum	-11 32 2	4.25	0.890		

Left insula	-24 -27 8	4.14	0.880
Right subgenual frontal cortex	4 19 -13	4.13	0.880
Right caudate	14 14 16	4.08	0.870
Right middle frontal gyrus	16 38 -5	3.98	0.860
Right thalamus	14 -23 -1	3.97	0.860
Left superior parietal gyrus	-36 -39 45	3.9	0.860
Left insula	-34 -26 -5	3.87	0.850
Right substantia nigra	8 -14 -11	3.76	0.840
Right superior frontal gyrus	4 29 52	3.75	0.840
Right precentral gyrus	7 -16 60	3.75	0.840
Left thalamus	-9 -19 -5	3.75	0.840
Right inferior frontal gyrus	61 18 15	2.4	0.630
Right precentral gyrus	62 9 15	1.81	0.490

Clusters of voxel-wise positive correlations between ^{18}F-flutemetamol and ^{18}F-AV1451 in MCI and AD subjects (clusters > 1000 voxels only)

Funding:

The PET scans and MRI scans were funded by the Medical Research Council (grant number WMCN_P33428) and part of the study was funded by Alzheimer's Research UK (grant number WMCN_P23750), while amyloid tracer was made available by GE Healthcare. ^{18}F-AV1451 PET scans were performed under licence from Avid.

Conflicts of interest:

Dr. Edison was funded by the Medical Research Council and now by Higher Education Funding Council for England (HEFCE). He has also received grants from Alzheimer's Research, UK, Alzheimer's Drug Discovery Foundation, Alzheimer's Society, UK, Novo Nordisk and GE Healthcare. He is also an external consultant to Pfizer. Prof. Brooks has received research grants and non-financial support from the Medical Research Council, grants from Alzheimer's Research Trust, during the conduct of the study; other from GE Healthcare, personal fees from AstraZeneca, Cytox, Shire, Novartis, GSK, Navidea, UCB, and Acadia, along with grants from Michael J Fox Foundation, European Commission, the Danish council for Independent Research, and the Lundbeck Foundation outside the submitted work.

Acknowledgements:

The authors thank Imanova Centre for Imaging Sciences, Imperial College Clinical Imaging facility and GE Healthcare for the provision of radiotracers, scanning and blood analysis equipment. We thank Avid pharmaceuticals for use of the radiotracer ^{18}F-AV1451. The PET scans and MRI scans were funded by the Medical Research Council and Alzheimer's Research UK. This article presents independent research funded by Medical Research Council and Alzheimer's Research, UK and supported by the NIHR CRF and BRC at Imperial College Healthcare NHS Trust.

Figure legends and captions

Figure 1: Voxel level increases in ^{18}F-flutemetamol and ^{18}F-AV1451 in the MCI and AD groups compared to the controls

Figure 2: Individual subject increases in amyloid and tau in the MCI group

Figure 3: Voxel level correlations between amyloid deposition and tau aggregation in MCI and AD

References

[1] Perl DP (2010) Neuropathology of Alzheimer's Disease. *Mt Sinai J Med* **77**.

[2] Braak H, Braak E (1991) Neuropathological Staging of Alzheimer Related Changes in Alzheimer's Disease. *Acta Neuropathol* **82**, 239-259.

[3] Crary JF, Trojanowski JQ, Schneider JA, Abisambra JF, Abner EL, Alafuzoff I, Arnold SE, Attems J, Beach TG, Bigio EH, Cairns NJ, Dickson DW, Gearing M, Grinberg LT, Hof PR, Hyman B, Jellinger K, Jicha GA, Kovacs GG, Knopman DS, Kofler J, Kukull WA, Mackenzie IR, Masliah E, McKee A, Montine TJ, Murray ME, Neltner JH, Santa-Maria I, Seeley WW, Troncoso JC, Vonsattel JP, White CL, 3rd, Wisniewski T, Woltjer RL, Yamada M, Nelson PT (2014) Primary age-related tauopathy (PART): a common pathology is associated with human aging. *Acta Neuropathol* **128**.

[4] Braak H, Del Tredici K (2011) The pathological process underlying Alzheimer's disease in individuals under thirty. *Acta Neuropathol* **121**, 171-181.

[5] Chien DT, Bahri S, Szardenings AK, Walsh JC, Mu F, Su MY, Shankle WR, Elizarov A, Kolb HC (2013) Early clinical PET imaging results with the novel PHF-tau radioligand [F-18]-T807. *J Alzheimers Dis* **34**, 457-468.

[6] Casanova R, Ryali S, Baer A, Laurienti PJ, Burdette JH, Hayasaka S, Flowers L, Wood F, Maldjian JA (2007) Biological Parametric Mapping: A Statistical Toolbox for Multi-Modality Brain Image Analysis. *Neuroimage* **34**, 137-143.

[7] Petersen RC, Caracciolo B, Brayne C, Gauthier S, Jelic V, Fratiglioni L (2014) Mild cognitive impairment: a concept in evolution. *J Intern Med* **275**, 214-228.

[8] McKhann GM, Drachman D, Folstein M, Katzman R, Price D, E.M. S (1984) Clinical diagnosis of Alzheimer's disease: report of the NINCDS-ADRDA Work Group under the auspices of the Department of Healthy and Human Services Task Force on Alzheimer's Disease. *Neurology* **34**, 939-944.

[9] McKhann GM, Knopman DS, Chertkow H, Hyman B, Jack C, Kawas C, Klunk W, Koroshetz WJ, Rossor M, Scheltens P, Carillo M, Thies B, Weintraub S, Phelps CH (2011) The diagnosis of dementia due to Alzheimer's disease: recommendations from the National Institute on Aging and the Alzheimer's Association workgroup. *Alzheimers Dement* **7**, 263-269.

[10] Hammers AA, R; Koepp, M; Free, S; Myers, R; Lemieux, L; Mitchell, T; Brooks, DJ; Duncan, JS (2003) Three-dimensional maximum probability atlas of the human brain, with particular reference to the temporal lobe. *Hum Brain Mapp* **19**, 224-247.

[11] Jack CR, Jr., Wiste HJ, Weigand SD, Therneau TM, Lowe VJ, Knopman DS, Gunter JL, Senjem ML, Jones DT, Kantarci K, Machulda MM, Mielke MM, Roberts RO, Vemuri P, Reyes DA, Petersen RC (2016) Defining imaging biomarker cut points for brain aging and Alzheimer's disease. *Alzheimers Dement* 13(3):205-216

[12] Gomez-Isla (1997) Neuronal Loss Correlates with but Exceeds Neurofibrillary Tangles in Alzheimer's Disease. *Ann Neurol* **41**, 17-24.

[13] Ingelsson M, Fukumoto H, Newell K, Growdon J, Hedley-White E, Frosch M, Albert M, Hyman B, Irizarry M (2004) Early Abeta accumulation and progressive synaptic loss, gliosis and tangle formation in AD brain. *Neurology* **62**, 925-931.

[14] Grundke-Iqbal I, Iqbal K, George L, Tung Y-C, Kim KS, Wisniewski HM (1989) Amyloid protein and neurofbrillary tangles coexist in the same neuron in Alzheimer disease. *Proc Natl Acad Sci U S A* **86**, 2853-2857.

[15] Hu W, Zhang X, Tung YC, Xie S, Liu F, Iqbal K (2016) Hyperphosphorylation determines both the spread and the morphology of tau pathology. *Alzheimers Dement* **12**, 1066-1077.

[16] Pooler AM, Polydoro M, Maury EA, Nicholls SB, Reddy SM, Wegmann S, William C, Saqran L, Cagsal-Getkin O, Pitstick R, Beier DR, Carlson GA, Spires-Jones TL, Hyman BT (2015) Amyloid accelerates tau propagation and toxicity in a model of early Alzheimer's disease. *Acta Neuropathol Commun* **3**, 14.

[17] Choi SH, Kim YH, Hebisch M, Sliwinski C, Lee S, D'Avanzo C, Chen H, Hooli B, Asselin C, Muffat J, Klee JB, Zhang C, Wainger BJ, Peitz M, Kovacs DM, Woolf CJ, Wagner SL, Tanzi RE, Kim DY (2014) A three-dimensional human neural cell culture model of Alzheimer's disease. *Nature* **515**, 274-278.

[18] Vasconcelos B, Stancu IC, Buist A, Bird M, Wang P, Vanoosthuyse A, Van Kolen K, Verheyen A, Kienlen-Campard P, Octave JN, Baatsen P, Moechars D, Dewachter I (2016) Heterotypic seeding of Tau fibrillization by pre-aggregated Abeta provides potent seeds for prion-like seeding and propagation of Tau-pathology in vivo. *Acta Neuropathol* **131**, 549-569.

[19] Ittner LM, Ke YD, Delerue F, Bi M, Gladbach A, van Eersel J, Wolfing H, Chieng BC, Christie MJ, Napier IA, Eckert A, Staufenbiel M, Hardeman E, Gotz J (2010) Dendritic function of tau mediates amyloid-beta toxicity in Alzheimer's disease mouse models. *Cell* **142**, 387-397.

[20] Dai CL, Hu W, Tung YC, Liu F, Gong CX, Iqbal K (2018) Tau passive immunization blocks seeding and spread of Alzheimer hyperphosphorylated Tau-induced pathology in 3 x Tg-AD mice. *Alzheimers Res Ther* **10**, 13.

[21] Dai CL, Tung YC, Liu F, Gong CX, Iqbal K (2017) Tau passive immunization inhibits not only tau but also Abeta pathology. *Alzheimers Res Ther* **9**, 1.

[22] Lockhart SN, Scholl M, Baker SL, Ayakta N, Swinnerton KN, Bell RK, Mellinger TJ, Shah VD, O'Neil JP, Janabi M, Jagust WJ (2017) Amyloid and tau PET demonstrate region-specific associations in normal older people. *Neuroimage* **150**, 191-199.

[23] Pontecorvo MJ, Devous MD, Sr., Navitsky M, Lu M, Salloway S, Schaerf FW, Jennings D, Arora AK, McGeehan A, Lim NC, Xiong H, Joshi AD, Siderowf A, Mintun MA, investigators FA-A (2017) Relationships between flortaucipir PET tau binding and amyloid burden, clinical diagnosis, age and cognition. *Brain*.

[24] Enatsu R, Gonzalez-Martinez J, Bulacio J, Kubota Y, Mosher J, Burgess RC, Najm I, Nair DR (2015) Connections of the limbic network: a corticocortical evoked potentials study. *Cortex* **62**, 20-33.

[25] Lacruz ME, Garcia Seoane JJ, Valentin A, Selway R, Alarcon G (2007) Frontal and temporal functional connections of the living human brain. *Eur J Neurosci* **26**, 1357-1370.

[26] Ittner LM, Gotz J (2011) Amyloid-beta and tau--a toxic pas de deux in Alzheimer's disease. *Nat Rev Neurosci* **12**, 65-72.

[27] Marquie M, Normandin MD, Vanderburg CR, Costantino IM, Bien EA, Rycyna LG, Klunk WE, Mathis CA, Ikonomovic MD, Debnath ML, Vasdev N, Dickerson BC, Gomperts SN, Growdon JH, Johnson KA, Frosch MP, Hyman BT, Gomez-Isla T (2015) Validating novel tau positron emission tomography tracer [F-18]-AV-1451 (T807) on postmortem brain tissue. *Ann Neurol* **78**, 787-800.

[28] Ikonomovic MD, Abrahamson EE, Price JC, Mathis CA, Klunk WE (2016) [F-18]AV-1451 positron emission tomography retention in choroid plexus: More than "off-target" binding. *Ann Neurol* **80**, 307-308.

[29] Hansen AK, Knudsen K, Lillethorup TP, Landau AM, Parbo P, Fedorova T, Audrain H, Bender D, Ostergaard K, Brooks DJ, Borghammer P (2016) In vivo imaging of neuromelanin in Parkinson's disease using 18F-AV-1451 PET. *Brain* **139**, 2039-2049.

[30] Thal DR, Beach TG, Zanette M, Heurling K, Chakrabarty A, Ismail A, Smith AP, Buckley C (2015) [(18)F]flutemetamol amyloid positron emission tomography in preclinical and symptomatic Alzheimer's disease: specific detection of advanced phases of amyloid-B pathology. *Alzheimers Dement* **11**, 975-985.

[31] Braak H, Del Tredici K (2014) Are cases with tau pathology occurring in the absence of Abeta deposits part of the AD-related pathological process? *Acta Neuropathol* **128**, 767-772.

[32] Duyckaerts C, Braak H, Brion J-P, Buee L, Del Tredici K, Goedert M, Halliday GM, Neumann H, Spillantini MG, Tolnay M, Uchihara T (2015) PART is part of Alzheimer disease. *Acta Neuropathol* **129**, 749-756.

[33] Villemagne V, Burnham S, Bourgeat P, Brown B, Ellis K, Salvado O, Szoeke C, Macauley S, Martins R, Maruff P, Rowe C, Masters C (2013) Amyloid B deposition, neurodegeneration, and cognitive decline in sporadic Alzheimer's Disease: a prospective cohort study. *Lancet* **12**, 357-367.

[34] Braak H, Braak E (1997) Frequency of Stages of Alzheimer-Related Lesions in Different Age Categories. *Neurobiol Aging* **18**, 351-357.

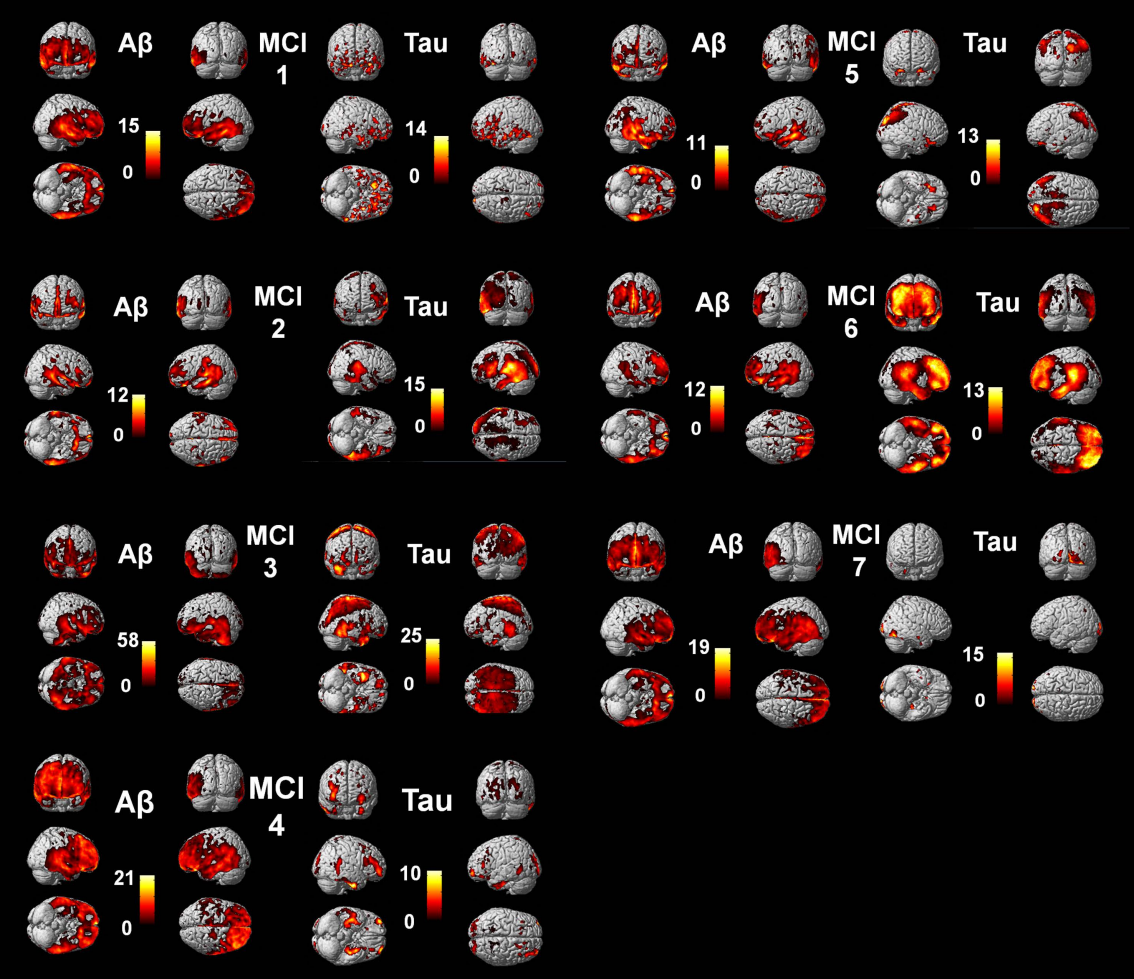
Aβ
MCI 1
Tau
15
0
14
0
Aβ
MCI 5
Tau
11
0
13
0
Aβ
MCI 2
Tau
12
0
15
0
Aβ
MCI 6
Tau
12
0
13
0
Aβ
MCI 3
Tau
58
0
25
0
Aβ
MCI 7
Tau
19
0
15
0
Aβ
MCI 4
Tau
21
0
10
0

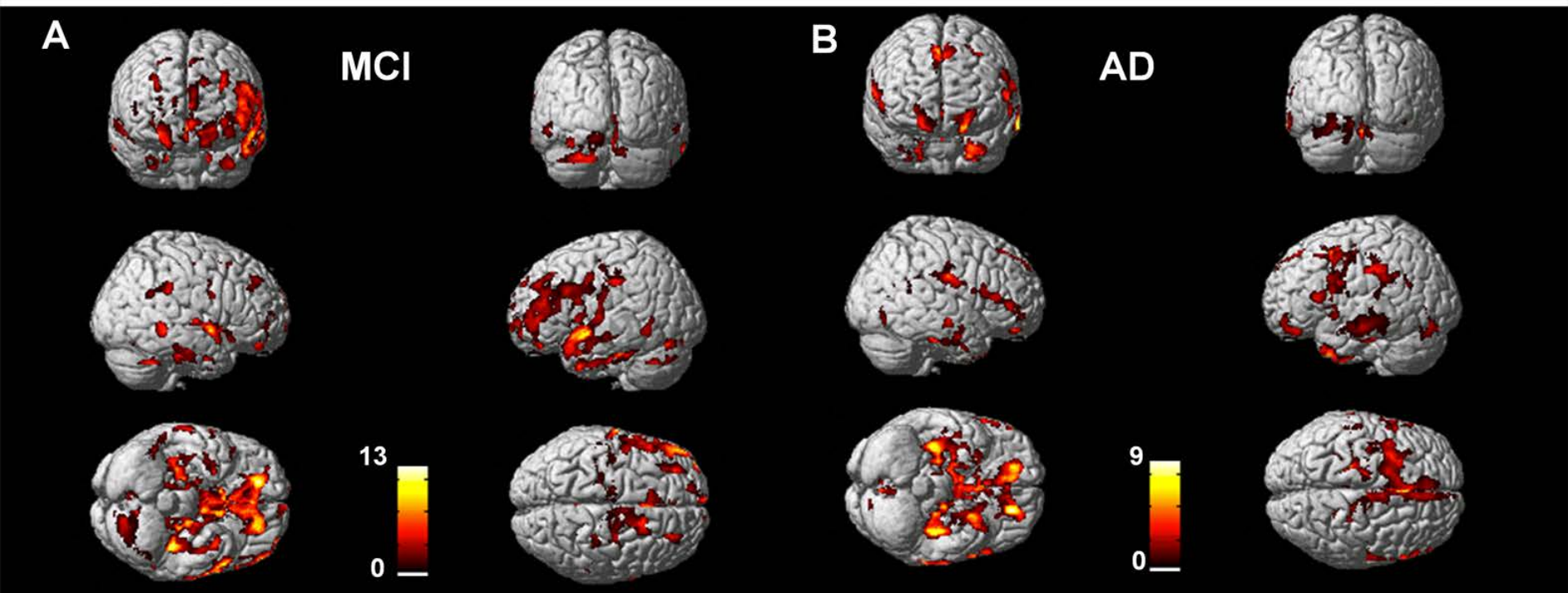
A
MCI
13
0
B
AD
9
0

Supplementary information

Supplementary Figure 1: Individual SUVR values for ^{18}F-flutemetamol binding in MCI and AD compared to the controls

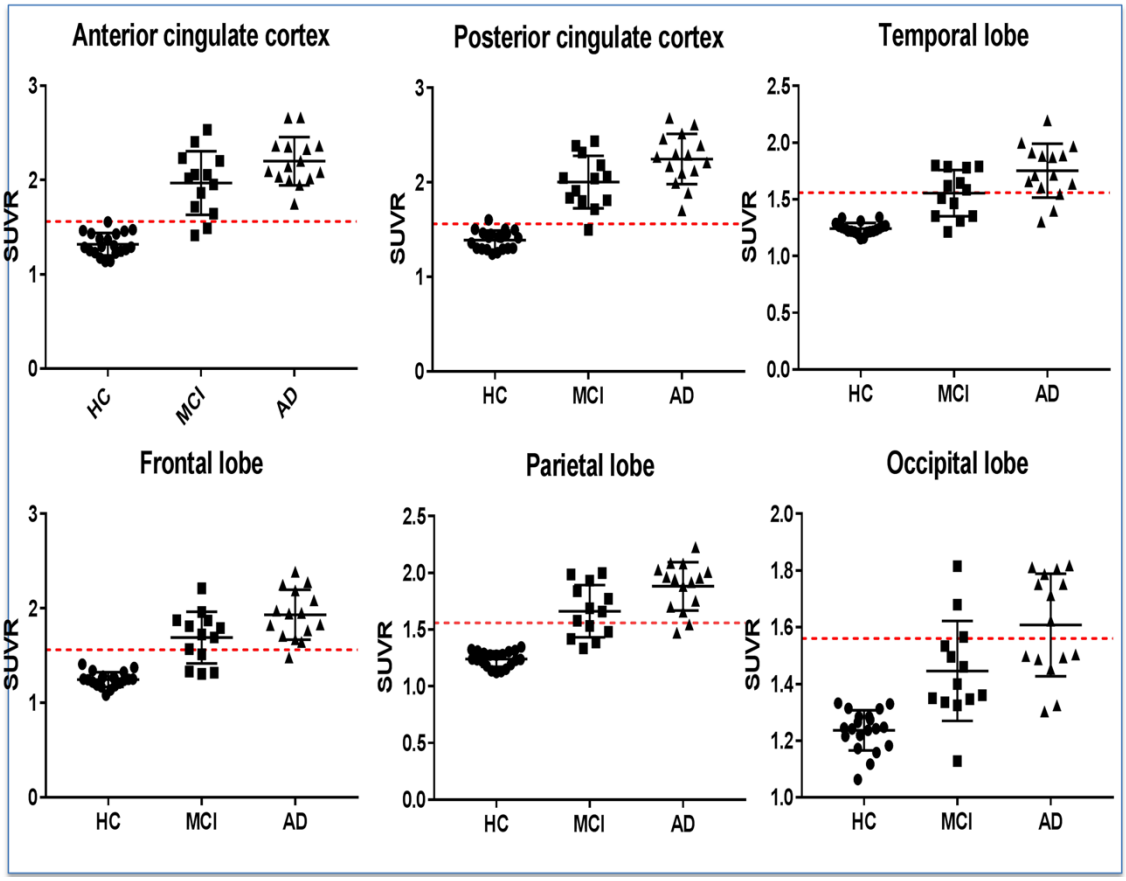

Supplementary figure 2: Individual SUVR values for ^{18}F-AV1451 binding in MCI and AD compared to the controls.

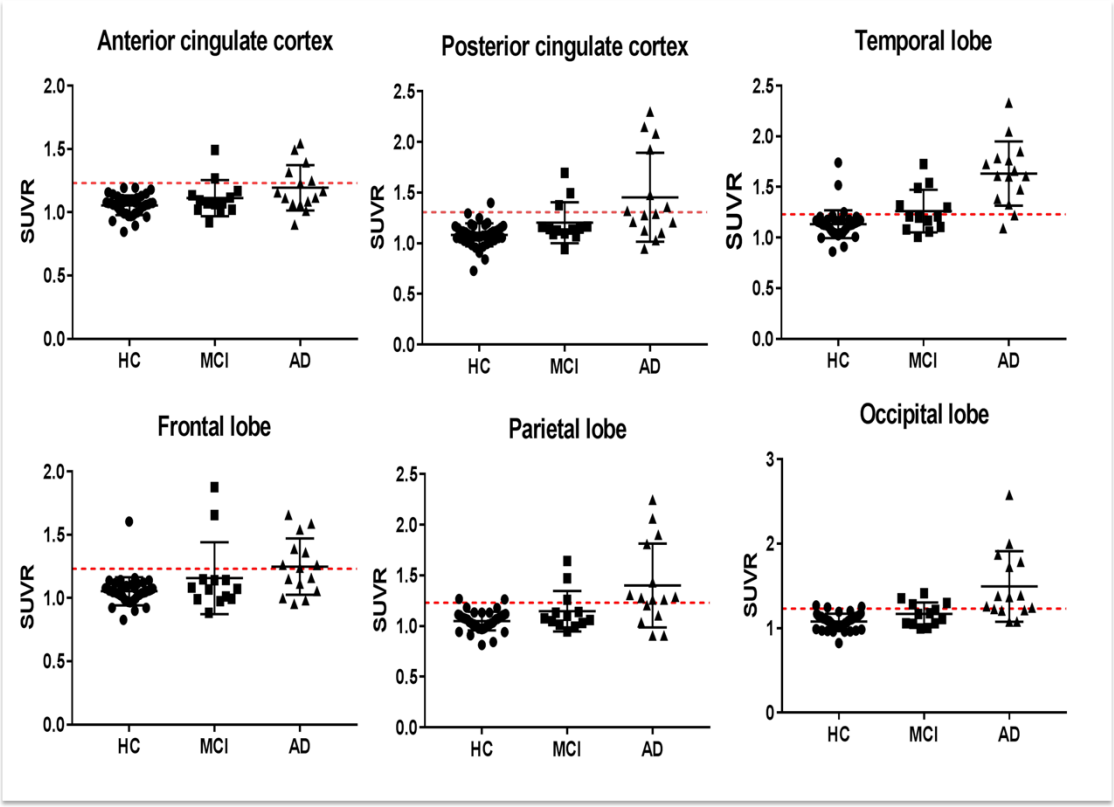

Supplementary figure 3: Individual SUVR values for 18F-AV1451 and 18F-AV45 for the healthy controls recruited from the ADNI database.